Matter

CellPress

Article

Using Small-Angle Scattering and Contrast Matching to Understand Molecular Packing in Low Molecular Weight Gels

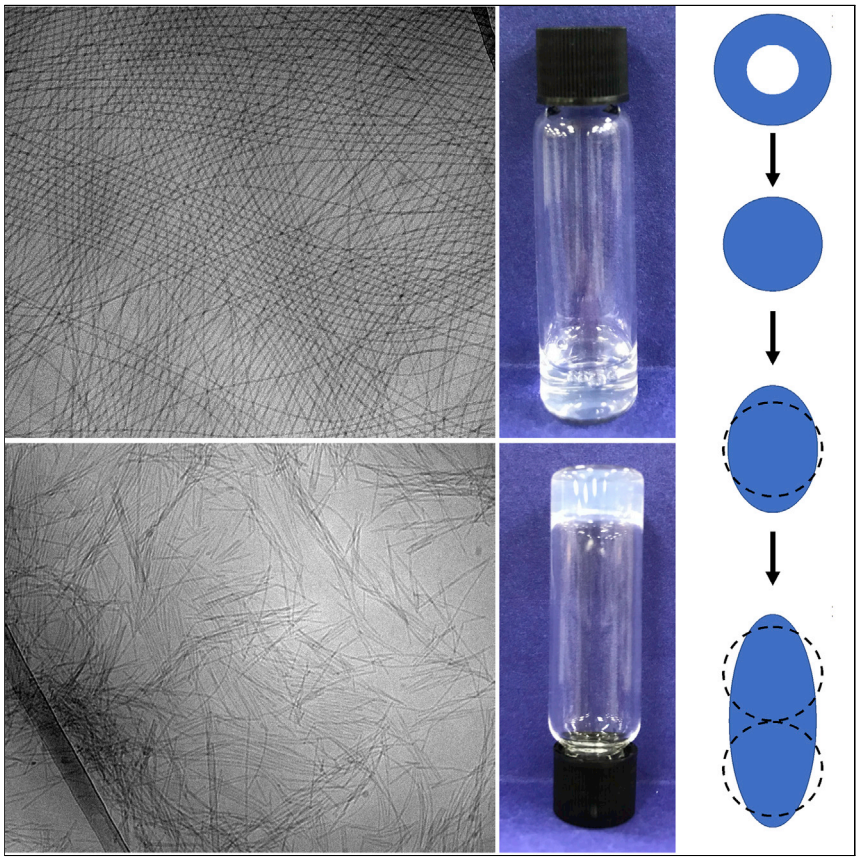

Gels can be formed by the self-assembly of small molecules into fibers that entangle and cross-link to form a network. Understanding how the molecules are packed in these self-assembled structures is difficult. Here, we use small-angle scattering to determine how the molecules pack in both the pre-gelled state and in the gel, as well as following the transition between the two types of aggregate.

Emily R. Draper, Bart Dietrich, Kate McAulay, ..., Ralf Schweins, Annela Seddon, Dave J. Adams

annela.seddon@bristol.ac.uk (A.S.)
dave.adams@glasgow.ac.uk (D.J.A.)

HIGHLIGHTS

We use small-angle scattering to understand supramolecular gels

In the pre-gelled state, the molecules pack into relatively well-ordered structures

When gels are formed, there is a lack of order in the final structures

The transition between aggregates can be followed by small-angle scattering

3 Understanding
Dependency and conditional studies on material behavior

Draper et al., Matter *2*, 764–778
March 4, 2020
https://doi.org/10.1016/j.matt.2019.12.028

Matter

CellPress

Article

Using Small-Angle Scattering and Contrast Matching to Understand Molecular Packing in Low Molecular Weight Gels

Emily R. Draper,[1] Bart Dietrich,[1] Kate McAulay,[1] Christopher Brasnett,[2] Haleh Abdizadeh,[3] Ilias Patmanidis,[3] Siewert J. Marrink,[3] Hao Su,[4] Honggang Cui,[4] Ralf Schweins,[5] Annela Seddon,[2,6,*] and Dave J. Adams[1,7,*]

SUMMARY

It is difficult to determine exactly the molecular packing in the aggregates in low molecular weight gels. Attempts to understand the packing have been made using X-ray diffraction, but there are complications with drying and questions as to whether the crystal structures represent the packing in the gel phase. Here, we exploit contrast matching in small-angle neutron scattering experiments. By preparing selectively deuterated analogs of the same molecule, the scattering from that section of the molecule decreases compared with the hydrogenated molecule. We examine packing in the pre-gelled solutions at high pH and in the gels at low pH. The data from the final gels show a lack of specific order in the aggregates that form the gel matrix. The packing in these systems is not well ordered in the gel state and so implies that it is likely that current models and cartoons are not correct.

INTRODUCTION

Low molecular weight gels are formed by the self-assembly of small molecules into anisotropic structures.[1–5] These gels are widely used in numerous applications,[6,7] including tissue engineering,[8] drug delivery,[9] optoelectronics,[10,11] structuring,[12] remediation,[13] and catalysis,[14] among others.

The small-molecule gelators self-assemble into structures such as fibers and nanotubes that are typically a few nanometers in diameter, but often micrometers in length. The gel network is formed when these structures entangle into a three-dimensional mesh that entraps the solvent. The properties of the gels result from the primary assembled structures, as well as how they entangle and cross-link. A key unanswered question in the field of low molecular weight gels is how the molecules pack in the primary self-assembled structures.[15] This is important because, without an understanding of this packing, it is difficult to design new gelators. In the main, the field is still heavily reliant on cartoons, which restricts progress.

The primary fiber structures can often be imaged by various microscopy techniques (although drying can be an issue[16] in terms of reproducing the 3D bulk conformation in solution, and furthermore, it is not evident how to probe a sample volume that is sufficiently statistically meaningful). However, microscopy does not usually have the resolution to allow an understanding of the molecular packing in the gel phase and so is most often used to understand the nature of the assembled structure. Techniques such as infrared (IR) spectroscopy or circular dichroism can inform us to

Progress and Potential

Small molecules can self-assemble into one-dimensional structures to give self-supporting gels. Such gels have a wide range of uses, including tissue engineering and drug delivery catalysis. It is difficult to understand how the molecules are packed in these structures, but this is hugely important if we are going to be able to learn from and design such materials.

Here, we use a combination of small-angle X-ray and small-angle neutron scattering with selectively deuterated molecules to understand the packing in the pre-gelled aggregates and in the gel state. We also use kinetic measurements to understand the transition between these aggregates. Our data show that there is a lack of order in the gel state, correlating with the limited predictive design rules in this field and with the importance of kinetics in forming the gel state. This approach allows us to understand our specific systems but represents a general approach that could be taken with different classes of gelator.

some degree about the intermolecular interactions, but they again do not provide all of the necessary information to understand this packing. In some cases, crystallography or powder X-ray diffraction is used on a dried gel.[17] This can be problematic; it is most commonly assumed that there are no changes on drying although mostly little proof is provided. There is accordingly a real need for new methods to understand and explain the molecular packing within the self-assembled structures.

A popular class of low molecular weight gelator (LMWG) is the functionalized oligopeptide.[18–21] Typically, the N terminus is functionalized with a large hydrophobic (usually aromatic) group such as fluorenylmethoxycarbonyl (Fmoc),[22] naphthalene,[23] pyrene,[24] carbazole,[25] indole[26] and phenothiazine,[27] among others.[28–30] The C terminus is usually free, meaning that hydrogels can be formed by dispersing the oligopeptide at high pH, where the carboxylic acid is deprotonated, and then decreasing the pH to re-protonate the C terminus. Gels are formed just below the apparent pK_a of the C terminus. There are many examples, with perhaps functionalized dipeptides being the most common.[19]

Despite the interest in this class of gelator, there is limited understanding of how the molecules pack in the gel phases. There has been some interpretation of crystal structures,[31] although we have shown that there is limited (if any) correlation between the crystal structures that can be obtained (even from the gel phase itself) and the diffraction data directly from the gel phase.[32] Indeed, there are a number of examples where this has been shown to be true for functionalized amino acids,[33] dipeptides,[32,34] and very recently a pentapeptide.[35] This leads us to question the value of such X-ray data in interpreting the packing and to highlight that, to our reading, the assumption that there is significant order in these systems has not been verified. We have further shown that there can be significant drying issues.[16] Unsurprisingly, there can be significant changes when gels are dried, which can include crystallization. Hence, in some cases where powder X-ray diffraction (pXRD) is used to demonstrate crystallinity and order, it can only be inferred that this is the case on drying, as opposed to necessarily demonstrating that this order exists in the gel phase.

There is one gelator for which the packing has been explained to some degree. This is FmocFF, perhaps the most famous of this class. The packing for FmocFF was explained on the basis of a range of data, including pXRD, circular dichroism, and IR data, and was suggested to lead to the formation of cylindrical structures using a specific π-β packing.[36] However, other reports find a different packing for the same gelator and describe conflicts in the first model[37] (e.g., different circular dichroism data[38]), and it has been shown that the packing is not the same in closely related gelators such as FmocAA.[39]

It is worth also pointing out that there are very few design rules for LMWGs, with many still being discovered by chance.[15,40] One school of thought suggests that the packing in the crystal state of the molecule (or more commonly closely related analogs) can be used to infer packing in the gel state,[41] although as stated above there are clear cases where this is not appropriate.[32] Aside from this approach, there are limited methods to fully understand molecular packing; although examples do exist that can probe packing to some degree, these only offer limited information. There is therefore significant interest in understanding the packing from the perspective of being able to rationally design future LMWGs.

Thus, there is a real need for the development of methods for understanding the packing in self-assembled aggregates. Here, we focus on this question and apply microscopic

[1]School of Chemistry, University of Glasgow, Glasgow G12 8QQ, UK

[2]School of Physics, HH Wills Physics Laboratory, University of Bristol, Tyndall Avenue, Bristol BS8 1TL, UK

[3]Groningen Biomolecular Sciences and Biotechnology Institute & Zernike Institute for Advanced Materials, University of Groningen, Groningen, the Netherlands

[4]Department of Chemical and Biomolecular Engineering, Whiting School of Engineering, Johns Hopkins University, 3400 North Charles Street, Baltimore, MD 21218, USA

[5]Large Scale Structures Group, Institut Laue-Langevin, 71 Avenue des Martyrs, CS 20156, 38042 Grenoble Cedex 9, France

[6]Bristol Centre for Functional Nanomaterials, HH Wills Physics Laboratory, University of Bristol, Tyndall Avenue, Bristol BS8 1TL, UK

[7]Lead Contact

*Correspondence: annela.seddon@bristol.ac.uk (A.S.), dave.adams@glasgow.ac.uk (D.J.A.)

https://doi.org/10.1016/j.matt.2019.12.028

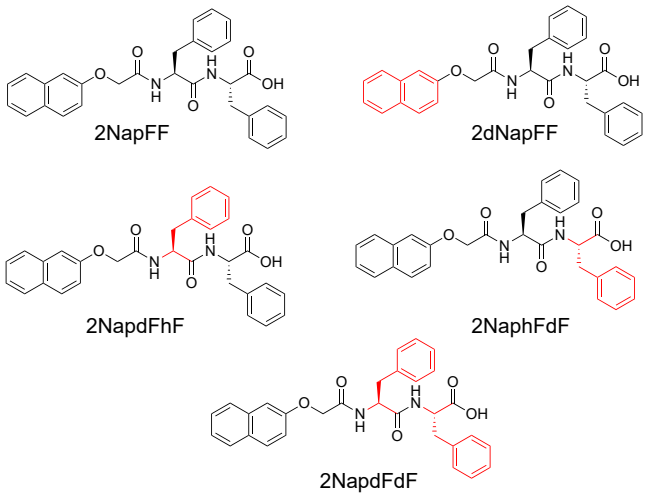

Figure 1. Chemical Structures of 2NapFF, 2dNapFF, 2NapdFhF, 2NaphFdF, and 2NapdFF
The deuterated sections in each are shown in red.

and small-angle scattering approaches. We combine small-angle X-ray scattering (SAXS) with small-angle neutron scattering (SANS) contrast-matching experiments to access information about the molecular packing; this approach is widely used in the surfactant literature[42–45] as well as (for example) structure determination in protein and polymer systems.[46–49] We start by describing a single well-studied and robust LMWG, 2NapFF (Figure 1). We have shown that this molecule forms self-assembled aggregates at high pH;[50,51] gels can be formed by reduction in the pH.[23] By preparing selectively deuterated analogs of the same molecule, the excess scattering from that section of the molecule is decreased compared with its hydrogenated analog in solution. Direct comparison of the scattering, as well as by fitting the data to models, allows us to understand how the molecules pack under different conditions. We then show that the approach can be used for two other examples.

RESULTS AND DISCUSSION

We have previously described the self-assembly of 2NapFF in detail (the chemical structure is shown in Figure 1). 2NapFF self-assembles at high pH (pH 10–11) into long anisotropic structures.[50] These entangle to give viscous solutions. The assembly is concentration dependent, as would be expected for a surfactant-like structure; the anisotropic structures are formed above 0.8 mg/mL.[50] These solutions can be gelled by a decrease in pH.[23]

We synthesized five analogs of 2NapFF (Figure 1). In addition to the parent molecule (2NapFF), we prepared 2dNapFF (where the naphthalene ring is deuterated but the dipeptide is hydrogenated), 2NapdFhF and 2NaphFdF (where the naphthalene is hydrogenated and either the first or second amino acid is deuterated, respectively), and 2NapdFdF (where the naphthalene is protonated and both amino acids are deuterated). All five were prepared using the same synthetic procedures (see Supplemental Information). For 2dNapFF, the deuteron at the 1 position of the naphthalene system is exchanged for a proton early in the synthetic sequence. The exchange is approximately 50:50 in the d_7/d_6-2-naphthoxyacetic acid *tert*-butyl ester and is complete in d_6-2-naphthoxyacetic acid; the NMR integral for the H-1 proton is unity and no d_7-compound was observed in the mass spectrum (see Supplemental Information, Figure S27). Although the deuteron at the 1 position is lost, six of the seven available positions are still deuterated.

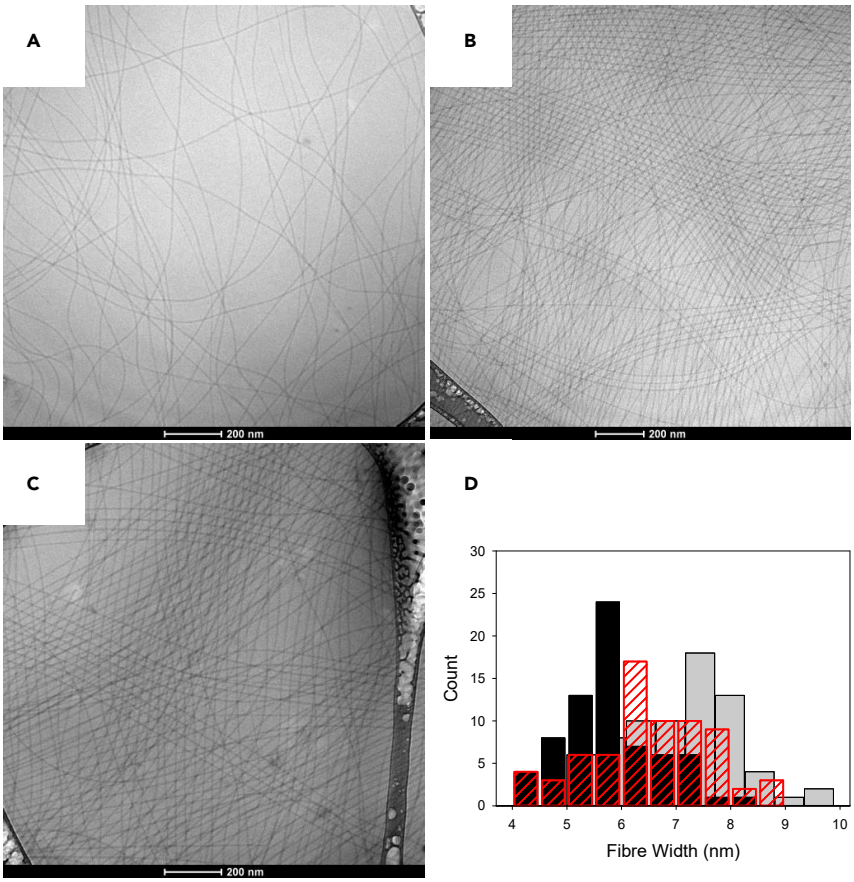

Figure 2. Cryo-TEM Data for Solutions of 2NapFF

(A–C) Cryo-TEM images of the solutions of (A) 2NapFF; (B) 2dNapFF; (C) 2NapdFF.
(D) The overlaid histogram of radii measured from at least 70 individual structures for each (2NapFF, dark gray; 2dNapFF, black; 2NapdFdF, red). Further images are shown in Figure S3 (Supplemental Information). For (A–C), the scale bars represent 200 nm in each case.

Packing in the Solution State

Solutions were prepared of all analogs in 100% D_2O at a concentration of 10 mg/mL. Cryo-transmission electron microscopy (TEM) images were collected for exemplar solutions of 2NapFF, 2dNapFF, and 2NapdFdF (Figure 2). In all cases, long anisotropic structures were imaged. Image analysis showed that the diameters of these structures were similar in all cases (6.87 $\pm$ 1.15, 5.85 $\pm$ 0.84, and 6.51 $\pm$ 1.09 nm, respectively). In addition, solutions of all five of these samples have similar viscosities (Figure S1, Supplemental Information), implying similar underlying structures.

We collected both SAXS and SANS data for the solutions. For SANS, it is usual to use D_2O as the solvent to maximize excess scattering of the hydrogenated structures. For direct comparison, SAXS was also carried out in D_2O on identical samples (Figure 3). The SAXS data[52] for 2NapFF at high pH can be fitted to a cylinder model (we have previously described how SAXS data for 2NapFF can be fitted to a flexible cylinder model; this is true here, but the fit to a cylinder model is similar in quality for 2NapFF and the fit to a cylinder model is much improved for the 2NapdFdF, so we focus on a single model here). The SAXS data for 2dNapFF and 2NapdFdF are similar to those of 2NapFF. The scattering data for all three of the solutions could be fitted to a cylinder model. The radii in all cases were similar (4.3, 4.0, and

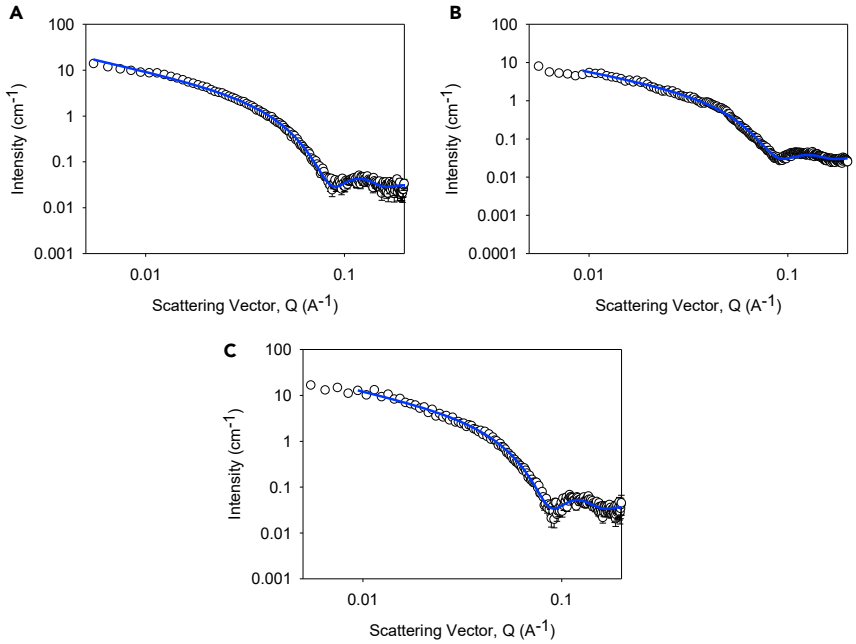

Figure 3. Small-Angle X-Ray Scattering Data for 2NapFF

Comparison of the SAXS data for (A) 2NapFF, (B) 2dNapFF, (C) 2NapdFdF at 10 mg/mL in D_2O. In all cases, the open circles show the data, and the blue lines are the fit to a cylinder model.

4.2 nm, respectively). A summary of the parameters extracted from the fits can be found in Table S1 (Supplemental Information). In all cases, the radii determined by SAXS are consistent with the cryo-TEM data.

We have previously discussed the SANS data for 2NapFF.[50,52] 2NapFF forms hollow cylinders at high pH. The data collected here are consistent with our previous work, and the SANS data for 2NapFF can be fitted to a hollow cylinder model combined with a power law, again as we have previously described.[50,52] The wall thickness is found to be 2.1 nm. The core radius (not detected by SAXS due to the lack of contrast) is found to be 1.65 nm. This means that the overall radius from the fit is 3.75 nm, slightly smaller, but close to that found from the fit to the flexible cylinder for the SAXS data. There is a discrepancy in length between SAXS and SANS. However, in both cases, the lengths are outside the *Q* range of the instrument, and so these values should be treated with caution (although considering the larger *Q* range of the SANS measurement, the values determined from these data are likely to be closer to the true values).

To further understand the molecular details of 2NapFF self-assembly, we performed atomistic molecular dynamics (MD) simulation of 2NapFF in water. MD is a powerful technique that, together with experiments, can be used to unravel the molecular packing of a large variety of supramolecular assemblies.[53–55] First, 200 ns unbiased simulations were carried out on a water box containing 300 randomly dispersed 2NapFF molecules. Filaments were formed, but not hollow structures, as suggested by the SANS experiments, mainly due to the limited length of the MD trajectory (see Supplemental Information Section 5). Thus, we resorted to biased MD simulations to ensure the formation of hollow tubular assemblies of 2NapFF monomers. In the biased simulations, cylindrical restraints were introduced to the system based on the profiles from the scattering data. By using cylindrical restraints, specific atoms are free to move along the axis and the circumference of a tube, while they are forced

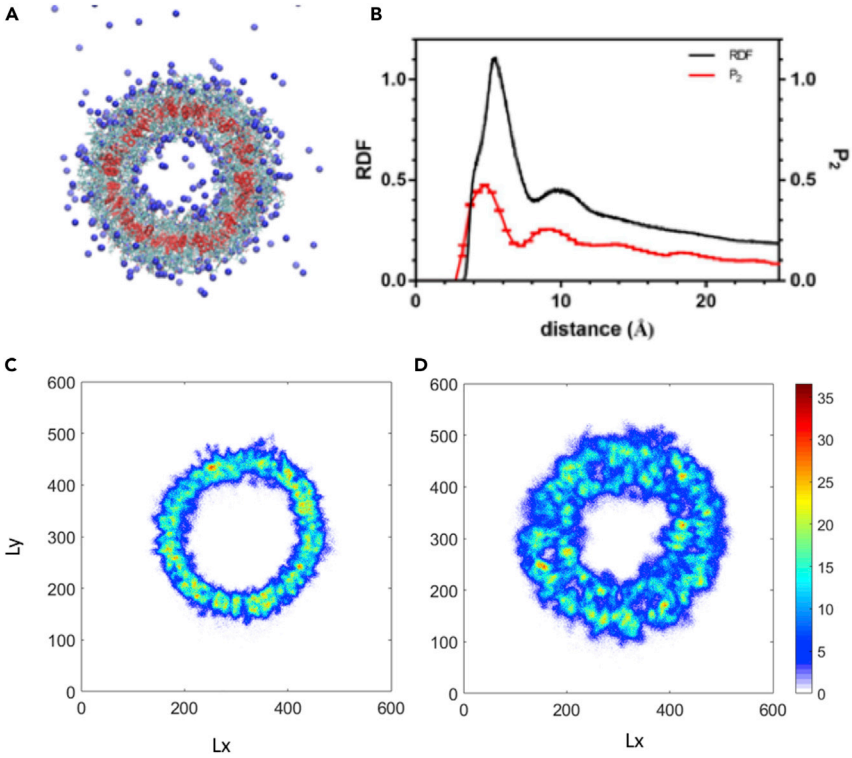

Figure 4. Atomistic Molecular Dynamics (MD) Simulations of 2NapFF

(A) Van der Waals representation of the preformed tube structure after 100 ns. The naphthalene rings are in red, phenylalanine close to naphthalene is in light blue, and terminal phenylalanine is in dark blue. Hydrogens, Na^+, and water not shown for clarity.

(B) Radial distribution function and P2 of naphthalene rings as a function of distance.

(C) Density map of naphthalene rings.

(D) Density map of phenylalanine rings in the tubes.

to stay within the designated areas. In the next step, we performed temperature annealing from 300 K to 400 K and back to 300 K to allow relaxation of the system. Finally, we removed the biasing force and ran MD simulations of the preformed tube for 100 ns (Figure S21, Supplemental Information).

The 100 ns MD simulation of the preformed tube reveals that the molecular structure of the tube stays stable while it loses its ordered stacking of the rings (Figure 4A). Na^+ ions and intramolecular hydrogen bonds stabilize the tube structure.

To get an insight into the molecular arrangement of the tube, we calculated the radial distribution function between the aromatic groups in the tube structure. The aromatic stacking is relatively flexible; although we found a few ordered stacks of the naphthalene rings locally, we also observed randomly oriented naphthalene rings distributed in different regions of the tube (Figure S22). The ordering of different aromatic groups was measured based on a second order parameter (P2) according to the angle formed between the normal to their planes. A P2 value close to 0 indicates random orientations, whereas a P2 value close to 1 indicates that the rings are parallel. In Figure 4B, we show that the naphthalene rings are mostly populated within 0.6 nm distance from any given naphthalene. However, the partially ordered naphthalene rings are within 0.4 nm distance from each other. Considering the size and dimension of naphthalene, we conclude that an off-set and slightly tilted arrangement is mostly adopted.

We calculated the partial mass density landscape of the preformed tube to show the most visited regions of the tube by either naphthalene or phenylalanine rings (Figures 4C and 4D). In highly populated areas of the landscape, we observed that naphthalene or phenylalanine rings tend to be in the middle and inner/outer layer, respectively. However, the phenylalanine rings adopt various conformations and visit the middle layer by folding and penetrating the naphthalene ring stacks. This smears out the density landscape to some extent and displays a population of phenylalanine rings in the middle layer of the density maps. We have quantified the extent to which the phenylalanine rings penetrate in between naphthalene rings by calculating the radial density of different rings (Figure S23). Since the cylinder does not have a perfect shape, the distribution of ring densities is not symmetric. Although the order of the peaks corresponds to the layered structure of the tube, there is an overlap between the radial density distribution of naphthalene rings and the two phenylalanine rings. We estimate that 20% of phenylalanine rings that are next to naphthalene penetrate in between naphthalene stacks. Only 5% of terminal phenylalanine rings fold back and reside within the naphthalene layers.

We now discuss the SANS contrast-matching experiments. As mentioned above, the deuterated section of the molecule scatters far less than the protonated section in D_2O. Assuming that the model shown in Figure 4 is correct, we would broadly expect the packing to correlate with the cartoon shown in Figure 5A. The terminal amino acid is shown in dark blue, the amino acid next to the naphthalene ring in light blue, and the naphthalene rings in red. Using contrast matching, we should conceptually be able to affect the intensity of scattering from these different segments of the molecule.

For 2dNapFF, where the naphthalene ring is deuterated, the shape of the scattering data is similar to that for 2NapFF. A hollow cylinder combined with a power law can again be used to provide a good fit to the data. The wall thickness and core radius are similar to those of 2NapFF (2.2 and 1.8 nm, respectively). Hence, the decrease in contrast from the naphthalene ring does not lead to a dramatic change in the scattering, implying that the naphthalene rings overlap and do not form a well-defined layer (in agreement with Figure 4C) or that the scattering from the amino acids dominates.

For 2NaphFdF, where the terminal phenylalanine (dark blue in Figure 5A) is deuterated, a hollow cylinder combined with a power law can again be used to fit the data. The wall thickness and core radius are different to those for 2NapFF (1.7 and 2.1 nm, respectively). Hence, the radius has increased by 0.3 nm and the thickness decreased by 0.4 nm, consistent with the loss of scattering from the terminal amino acid (dark blue in Figure 5A).

For 2NapdFhF, a hollow cylinder combined with a power law again provides a good fit to the data. The fit implies that the wall thickness and core radius appear to be similar to those in 2NapFF (2.1 and 1.8 nm, respectively). This implies diffuse packing of structure smearing out the scattering, and so we do not see a well-defined onion-like structure as might be expected.

Finally, the scattering intensity from 2NapdFdF is significantly lower than that for 2NapFF. Nonetheless, the data can again be fitted to the hollow cylinder combined with a power law. From the fit, the cylinder is very thin, with a wall thickness of 0.5 nm and a radius of 2.4 nm. This agrees with the model, where in this case we should only be detecting the scattering from the naphthalene rings (red in Figure 5A). To access

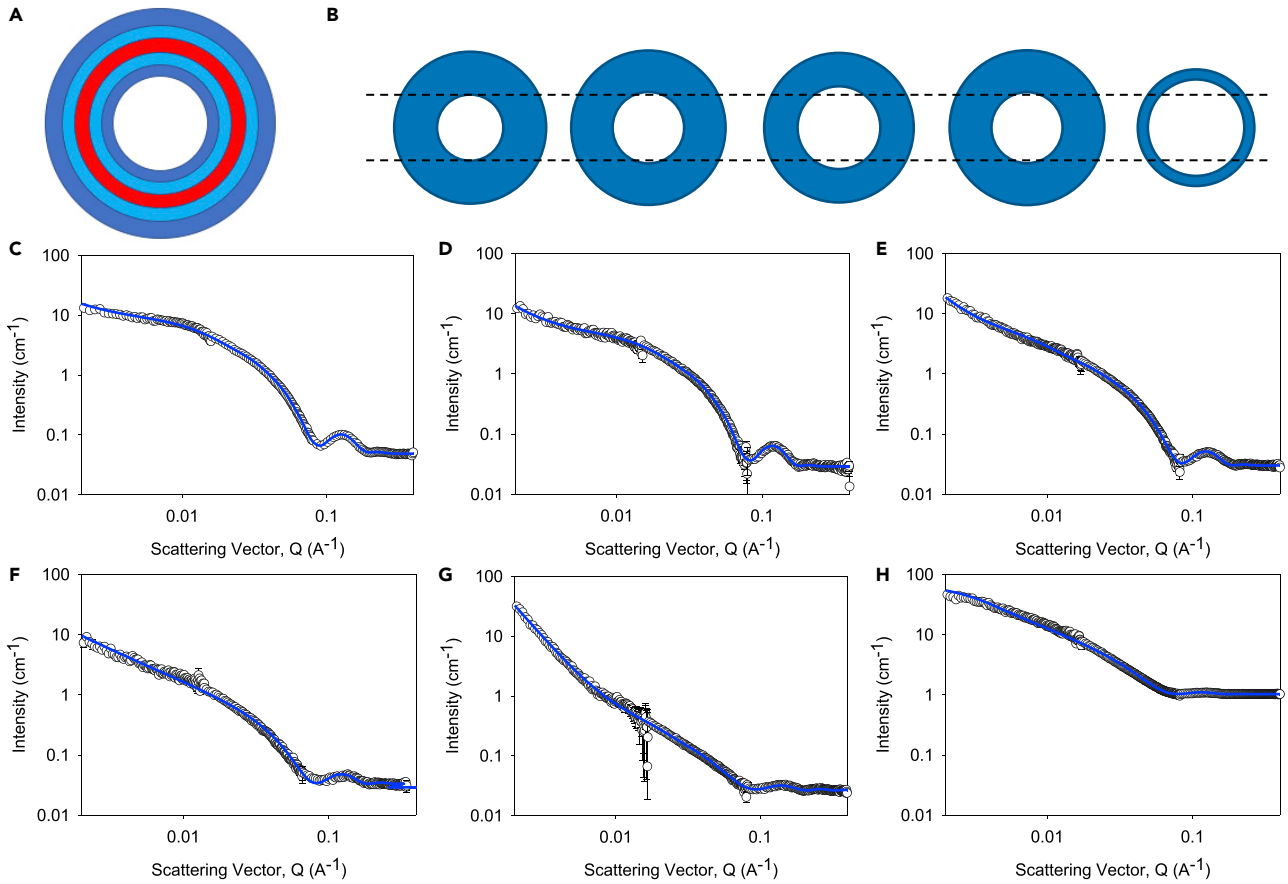

Figure 5. Contrast-Matching Small-Angle Neutron Scattering Data for 2NapFF

(A) Cartoon of structures formed by 2NapFF end on, with color coding for the different sections of 2NapFF (red, naphthalene ring; light blue, phenylalanine next to naphthalene; dark blue, terminal phenylalanine).

(B) End-on overview of structures formed from (from left to right) 2NapFF, 2dNapFF, 2NaphFdF, 2NapdFhF, and 2NapdFdF in D_2O on the basis of the fits to the SANS data in (C)–(G). The sizes are all scaled to the size derived from the fits to the SANS data. The horizontal dashed lines are provided as a guide to the eye and represent the inner radius of the fully hydrogenated 2NapFF.

(C) SANS data and fit for 2NapFF in D_2O.

(D) SANS data and fit for 2dNapFF in D_2O.

(E) SANS data and fit for 2NaphFdF in D_2O.

(F) SANS data and fit for 2NapdFhF in D_2O.

(G) SANS data and fit for 2NapdFdF in D_2O.

(H) SANS data and fit for 2NapdFdF in H_2O.

For (C)–(H), the data are shown as open circles and the fits to the data as blue lines.

more information here, we also carried out SANS for 2NapdFdF in H_2O. In this experiment, the contrast should now be such that the deuterated sections of the molecule should scatter. In line with this, the scattering is now very different (Figure 5H), and the data are best fit to a hollow cylinder, with a wall thickness of 2.5 nm, and a core radius of 1.7 nm, close to that found for 2NapFF in D_2O as expected.

Hence, from the SAXS and SANS scattering experiments on the solutions, it is clear that the molecules are assembling in a surfactant-like manner, such that the hollow cylinders are formed. Hydrophobic collapse presumably drives the assembly with the self-assembled structures being stabilized by the carboxylates. The contrast-matching experiments are consistent with the cartoon models shown in Figures 5A and 5B, and the same structures are formed for all deuterated and non-deuterated analogs.

Packing in Gels

Each of the solutions was gelled by decreasing the pH of the solutions. Again, all gels were prepared in D_2O to allow direct comparison. The initial pH (strictly pD) was also kept the same. To bring about gelation, we used the hydrolysis of glucono-δ-lactone (GdL)[56] as we have described elsewhere.[57] This results in a slow, uniform pH change and reproducible gels and has the advantage that it is possible to follow the gelation process with time. There were small differences in rheological profiles with time (Figure S2), but the final properties are similar. Due to the strengths of the gels, effective cryo-TEM could not be collected; the images collected show simply broken structures (e.g., Figure S4).

The SAXS data for the gels fit well to a flexible elliptical cylinder model. For the fitting, the lengths were fixed to be arbitrarily long and outside the *Q* range of the equipment. The radii were found to be 4.1, 4.1, and 3.6 nm for 2NapFF, 2dNapFF, and 2NapdFdF, respectively, with axis ratios of 2.5, 1.8, and 2.6, respectively. Hence, the radii are similar to the values for the structures at high pH (see above), but the structures are now elliptical as opposed to cylindrical.

At high pH, NMR data typically show around 20% of the expected integral of 2NapFF.[58] We interpret this as being due to the persistence of the micellar structures at high pH, with the molecules spending most of their time in the aggregated stated. Since only the molecularly dissolved 2NapFF is detectable by NMR, this results in a lower than expected integral.[59] As the pH decreases, the 2NapFF becomes less soluble. Thus, we would expect the time the molecules spend in the aggregated state to increase as the pH decreases. Hence, it seems unlikely that there is an initial solubilization and then re-aggregation, but rather that there is a direct structural transition as the pH decreases.

In terms of how the structural transition occurs, initially we focus on 2NapFF. One advantage of using GdL to adjust the pH is that the slow hydrolysis allows time-resolved experiments. Since the hydrolysis is so reproducible, it is possible to carry out the SANS experiments such that data at different camera lengths can be independently collected and added together. Using this method, time-resolved SANS experiments show that the peak arising from the hollow core for 2NapFF disappears quickly (within the first 15 min, Figure S6A; kinetic runs were also collected at high *Q* only, which makes the data difficult to fit, but does show that the peak from the hollow core begins to disappear as soon as the pH starts to drop, Figure S6B). For 2NapFF, pH titrations have shown previously that there are two apparent pK_a values, despite there being only a single ionizable group.[52] We have interpreted this as being due to structural transitions as the pH is decreased. In light of the time-resolved SANS data, we hypothesize that the carboxylic acids in the interior of the hollow cylinder have a higher apparent pK_a than those on the outside of the cylinders. Thus, as the pH decreases, the interior first becomes protonated and leads to a structural change. The pH data with time (Figure S7) are consistent with this. After 15 min, when the peak due to the core has disappeared, the fit to the data is best achieved using a flexible cylinder model combined with a power law, giving a radius of 2.9 nm (Figure S8 and Table S4).

Following this, as the pH is decreased further, ellipticity begins to occur, as shown by the fit to a flexible cylinder model combined with a power law becoming steadily worse (as shown by an increase in the chi-squared value). In addition, the scattering intensity at mid-*Q* increases with time. The data at 3 h can be best fit to a flexible elliptical cylinder with a radius of 2.9 nm and an ellipticity of 1.5. After 24 h, the data can be best fit to a flexible elliptical cylinder with a radius of 2.7 nm and an ellipticity of 2.4 (Figure S9 and Table S5).

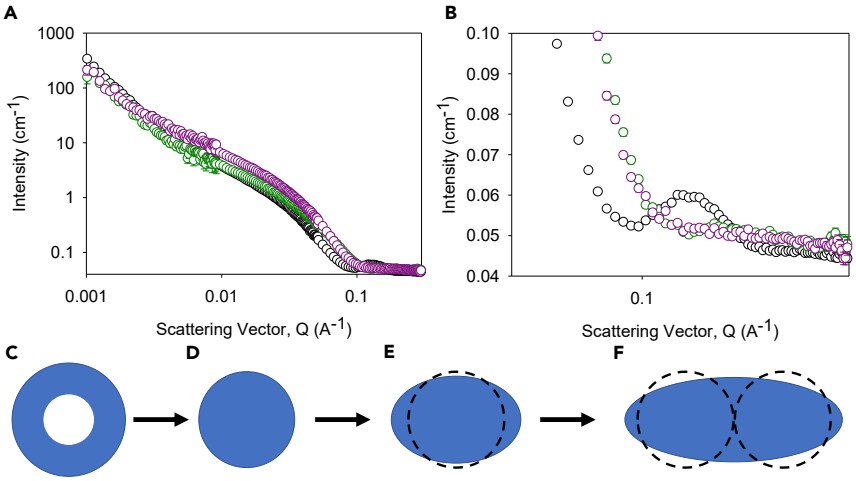

Figure 6. Small-Angle Scattering Data over Time during Gelation

(A) SANS for 2NapFF before addition of GdL (black), 15 min after addition (green), and 180 min after addition (purple).

(B–F) Expansion of the data in (A) to show the disappearance of the peak at high Q (B). As the pH is decreased, the hollow cylinders formed by 2NapFF (C) initially lose the core (D; fit to data at 15 min) before becoming elliptical (E; fit to data at 180 min). At 24 h, the ellipse is more pronounced (F; shown superimposed are two structures the size of those in C). In all cases, the cartoons are drawn to scale on the basis of the SANS data.

While the radius of one axis remains similar, the ellipticity gradually increases. The overall cross-sectional area is significantly greater in the elliptical structure than in the cylindrical structures formed at high pH (Figure 6). If we assume that there is a structural transition as discussed above, the apparent increase in cross-section could only come via significant shrinkage in the length (to maintain the absolute number of molecules per aggregate), which seems unlikely, or by the elliptical structure being a result of lateral association of cylindrical structures (Figure 6). This would also explain the gradual increase in ellipticity, with lateral association increasing with time (it seems likely to us that there is a mixture of individual and laterally associated structures, with an increase in the concentration of the laterally associated structures with time); fits to a cylinder model with polydispersity were not as good as using an elliptical model.

Hence, the best fit to the scattering data for the final gels formed by the addition of GdL to a solution of 2NapFF is obtained by considering the gel fibers to have a non-uniform cross-section and considering them as elliptical cylinders. Thus, in a Guinier plot of $\ln(Q^{\alpha}I(Q))$ versus Q^2, a value of $\alpha = 2$ will give the best linear fit at low Q. It is also possible to extract the thickness of the scattering objects from a plot of $\ln(Q^2I(Q))$ versus Q^2. For each sample presented here, the thickness was calculated using the linear region at very low Q.[60] These values are shown in Table S5. It is striking to note that the values for the deuterated samples are greater than for the non-deuterated sample, and that for 2NapdFdF, the dimensions of the scattering object are ~1.6 times that of 2NapFF. This differs from the fits to the SAXS data from the same structures, where the dimensions were not found to change. This apparent increase in the dimensions therefore seems to be a contrast effect.

Since the fits to the SAXS and SANS show that the gel fibers have an elliptical cross-section, we next performed fits of the SANS data for the deuterated samples to an elliptical cylinder model. To re-iterate the above, 2NapFF has been shown

previously to fit a flexible elliptical cylinder model, with a minor radius of 3 nm and an axis ratio of 2.6. In contrast, fits of the deuterated samples to a flexible elliptical cylinder model were unsuccessful; however, fits to an elliptical cylinder (with no Kuhn length component included) were more successful. It is not clear whether the difference in the models required to fit the data is due to a genuine stiffening of the deuterated samples, rendering them inflexible, or whether the degree of deuteration of the samples causes the fits to deviate from ideal. A polydispersity on the radius needed to be included with the fits to obtain the best values of the reduced chi-squared value

Values obtained from the fits show that in all cases the minor axis radius is approximately 4 nm, which is close to that seen for the overall radius of the cylinder in solution. The exception to this is 2NapdFdF, which appears to have a larger radius than is seen in the cylinder. However, the fibers are clearly elliptical, with axis ratio values of around 2.5, meaning that the major axis has a radius of around 10 nm. Comparing these values with the thickness obtained by the Guinier fits shows that in the case of 2NapFF and 2NaphFdF, the values obtained from the Guinier plot are close to the thickness of the short axis of the ellipse. However, for the 2dNapFF and 2NapdFhF samples, the thickness obtained from the Guinier plots is closer to the value obtained from the long axis of the ellipse. 2NapdFdF has a value for the short axis radius that is 5 nm, corelating with the thickness found from the Guinier plot. 2NapdFdF fits poorly over the whole Q range, and the only way to get anything approximating a decent fit is to cut the data at low Q. This is perhaps unsurprising, as the degree of deuteration in this sample means that scattering is only occurring from a thin "disc" of material, which may render the sample too unreliable to allow firm conclusions to be drawn. It should also be noted that these fits deviate at low Q, and thus, caution should be exercised in drawing inference from them. The deviation at low Q can be attributed to polydispersity within the sample (e.g., the presence of larger aggregates). A more detailed discussion of additional fitting of these data can be found in the Supplemental Information in Section 4.3.

From all of these scattering data, we can infer that deuteration does not affect the overall structures formed since the SAXS data are similar in each case. It is also worth highlighting that although cryo-TEM was difficult to collect due to sampling of these very rigid gels, the structures imaged are very similar for all 2NapFF variants (Figure S4). This again shows that deuteration does not affect the aggregation. However, the SANS data are more complex. What is clear, however, is that there is not well-defined packing. Instead, each gel can be best fit to an elliptical cylinder without clear contrast differences where the deuterated segments are packed, as we found above for the solution phase. Hence, these data imply that there is no well-defined packing in the gel phase. This might be initially surprising considering the (often implicit) assumption that such gels have a high degree of order.

To demonstrate that this method is not only viable for 2NapFF, we have also prepared samples of other gelators: 1ThNapFF (Figure 7A) and 2NapVG (Figure 7C). These were selectively deuterated, and SAXS and contrast-matching SANS were performed as described for 2NapFF. All fitting parameters and graphs of the SANS and SAXS data can be found in Section 4.4 in the Supplemental Information. At high pH, the SANS data for 1ThNapFF fits to a flexible cylinder with radius of 1.5 nm. The deuterated analog, 1ThNapdFdF similarly fits a flexible cylinder, but with a radius of 0.47 nm, reflective of the smaller effective cylinder radius seen by the neutrons (Figure 7B). The decrease in radius is consistent with the expected size of the diphenylalanine from the data above for 2NapFF (0.75 nm for 2NapFF

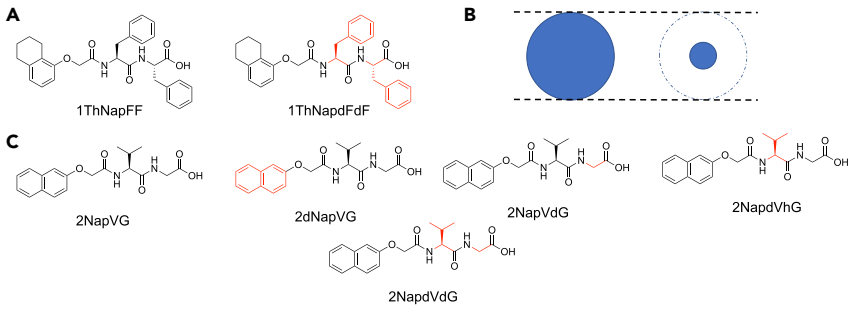

Figure 7. Chemical Structures and Assembly of 1ThNapFF and 2NapVG

(A) Chemical structures of 1ThNapFF and 1ThNapdFdF.

(B) End-on overview of structures formed at high pH from (left) 1ThNapFF and (right) 1ThNapdFdF on the basis of the fits to the SANS data (see Supplemental Information). The sizes are scaled to the sizes derived from the fits to the SANS data. The horizontal dashed lines are provided as a guide to the eye and show the external radius of the fully hydrogenated 1ThNapFF.

(C) Chemical structures of 2NapVG, 2dNapVG, 2NapVdGF, 2NapdVhG, and 2NapdVdG. For (A) and (C), the deuterated sections in each are shown in red.

and 1.03 nm for 1ThNapFF; the size is presumably affected by the absolute packing, but the values are close). These data are therefore consistent with 1ThNapFF forming worm-like micelles at high pH, where the tetrahydronaphthalenes form the core of the cylinders (Figure 7B). When the pH was lowered to form a gel, the scattering data for both 1ThNapFF and 1ThNapdFdF fitted well to the flexible elliptical cylinder model, with radii of 4.1 nm and 2.7 nm, respectively. The aspect ratios were found to be 2.3 for 1ThNapFF and 1.9 for 1ThNapdFdF. This again indicates, as for 2NapFF, that the SANS data are measuring structures that are larger in the gel state than in solution, presumably as a consequence of packing of multiple fibers as the pH is lowered. However, unlike 2NapFF, the value for the minor axis is larger in both the non-deuterated and deuterated sample, suggesting that the aggregation is more pronounced in this system. SAXS data collected on both 1ThNapFF and 1ThNapdFdF shows again the formation of flexible elliptical cylinders but here with aspect ratios and minor radii that are comparable with the sizes observed in the SANS data for the non-deuterated analog, showing that the deuteration is not affecting the structure. However, as for 2NapFF, there is no indication that there are sharp interfaces arising from contrast differences, implying again that there is not well-defined packing in the structures in the gel phase.

Unlike 2NapFF and 1ThNapFF, 2NapVG does not form well-defined aggregates at high pH, and the scattering is weak at this point, even for the fully hydrogenated molecule.[59] However, gels are formed when the pH is decreased. Hence, we repeated the scattering experiments for gels made from 2NapVG with varying degrees of deuteration (Figure 7A). Fitting parameters and graphs of SANS and SAXS data obtained can be found in Section 4.5 (Supplemental Information). At high pH, 2NapVG does not show any objects in solution that can be measured by scattering.[59] On lowering the pH, gels were formed. SAXS data of all samples could again be fitted to a flexible elliptical cylinder model with minor radius and axis ratio comparable with the SANS data collected from the non-deuterated 2NapVG. This again shows that the aggregation is not affected by the deuteration. For the SANS data, all cases fitted to a flexible elliptical cylinder model combined with a power law. The fits imply that there is little change in the radius at all degrees of deuteration apart from 2NapdVdG, where all data can be fitted with a radius of around 3.3 nm; the data for 2NapdVdG require a radius of 4.2 nm for an adequate fit. Hence, again we can see that there is no suggestion of order from the contrast-matching experiments.

Conclusions

We have shown that selective deuteration and contrast-matching experiments are a powerful approach to understanding the packing in aggregates formed by functionalized dipeptides at high pH. The data show that these dipeptides assemble as conventional surfactants at high pH. For 2NapFF, as the pH is decreased to form gels, the packing is disrupted; the hollow core is first lost to form cylindrical structures, which then laterally associate. Loss of the core undoubtedly means that the packing is disrupted. Combined with the lateral association of fibers, this means that the deuteration and contrast-matching approach does not allow fine detail of the packing to be assigned, which makes sense from this model. The lack of order arises from the pre-existence of structures at high pH and the slow pH change. The pH change results in collapse of the hollow cylinders and hence a lack of order. Similarly, 1ThNapFF aggregates in a surfactant-like manner at high pH, but no order is seen on gelation. 2NapVG, which does not form persistent structures at high pH, also shows no sign of order on gelation. Although this might be seen as a negative, we rather see this as indicative of further evidence that the packing in these systems is not well ordered in the gel state, and so implies that it is likely that current models and cartoons are not correct.

Conceptually, understanding the packing would allow molecular design such that specific functional groups could be placed in a specific location for a reaction for example. These data show the difficulty in understanding the packing in the gel state and imply that there may not in fact be well-defined packing. This correlates with the lack of crystalline order seen in these gels. The data also correlate with the difficulty in determining predictive design rules; if the packing is not well-defined, this implies that the kinetic profile to the gel state is important, which will not be captured in many predictive models.

Nonetheless, the demonstration of surfactant-like packing at high pH opens up the opportunity for further design. It should be able to change morphology by changing the packing parameter, for example, by varying counter ions. Further, we note that the difference in apparent pK_a inside and outside the 2NapFF nanotubes leading to the collapse of the core on gelation could be exploited in other ways.

EXPERIMENTAL PROCEDURES

Full experimental procedures are provided in the Supplemental Information.

SUPPLEMENTAL INFORMATION

Supplemental Information can be found online at https://doi.org/10.1016/j.matt.2019.12.028.

ACKNOWLEDGMENTS

D.J.A. thanks the EPSRC for a Fellowship (EP/L021978/1), which also funded K.M. and B.D. E.R.D. thanks the Leverhulme Trust for funding (ECF-2017-223) and the University of Glasgow for an LKAS Leadership Fellowship. The Ganesha X-ray scattering apparatus used for this research was purchased under EPSRC Grant "Atoms to Applications" (EP/K035746/1). The experiment at the Institut Laue-Langevin was allocated beam time under experiment numbers 9-11-1879 (https://doi.org/10.5291/ILL-DATA.9-11-1879), 9-11-1907 (https://doi.org/10.5291/ILL-DATA.9-11-1907), and 9-10-1304. We thank Beatrice Cattoz (University of Greenwich) for experimental assistance with experiment 9-10-1304. This work benefitted from the SasView software, originally developed by the DANSE project under NSF award DMR-0520547.

AUTHOR CONTRIBUTIONS

E.R.D., A.S., and D.J.A. designed the study. E.R.D., D.J.A., and R.S. designed and carried out the SANS experiments. B.D. and D.J.A. synthesized the molecules. K.M. carried out the viscosity and rheology work. C.B. and A.S. carried out the SAXS experiments. A.S. and D.J.A. fitted the scattering data. H.A., I.P., and S.J.M. performed the computational work. H.S. and H.C. carried out the cryo-TEM experiments. D.J.A. and A.S. wrote the initial draft of the paper, to which all authors contributed for the final manuscript.

DECLARATION OF INTERESTS

The authors declare no competing interests.

Received: June 21, 2019
Revised: November 1, 2019
Accepted: December 20, 2019
Published: January 29, 2020

REFERENCES

1. Terech, P., and Weiss, R.G. (1997). Low molecular mass gelators of organic liquids and the properties of their gels. Chem. Rev. *97*, 3133–3160.

2. Estroff, L.A., and Hamilton, A.D. (2004). Water gelation by small organic molecules. Chem. Rev. *104*, 1201–1218.

3. Draper, E.R., and Adams, D.J. (2017). Low-molecular-weight gels: the state of the art. Chem *3*, 390–410.

4. Amabilino, D.B., Smith, D.K., and Steed, J.W. (2017). Supramolecular materials. Chem. Soc. Rev. *46*, 2404–2420.

5. de Loos, M., Feringa, B.L., and van Esch, J.H. (2005). Design and application of self-assembled low molecular weight hydrogels. Eur. J. Org. Chem. *2005*, 3615–3631.

6. Hirst, A.R., Escuder, B., Miravet, J.F., and Smith, D.K. (2008). High-tech applications of self-assembling supramolecular nanostructured gel-phase materials: from regenerative medicine to electronic devices. Angew. Chem. Int. Ed. *47*, 8002–8018.

7. Dawn, A., Shiraki, T., Haraguchi, S., Tamaru, S.-I., and Shinkai, S. (2011). What kind of "soft materials" can we design from molecular gels? Chem. Asian J. *6*, 266–282.

8. Skilling, K.J., Citossi, F., Bradshaw, T.D., Ashford, M., Kellam, B., and Marlow, M. (2014). Insights into low molecular mass organic gelators: a focus on drug delivery and tissue engineering applications. Soft Matter *10*, 237–256.

9. Tian, R., Chen, J., and Niu, R. (2014). The development of low-molecular weight hydrogels for applications in cancer therapy. Nanoscale *6*, 3474–3482.

10. Christoff-Tempesta, T., Lew, A.J., and Ortony, J.H. (2018). Beyond covalent crosslinks: applications of supramolecular gels. Gels *4*, 40.

11. Fichman, G., and Gazit, E. (2014). Self-assembly of short peptides to form hydrogels: design of building blocks, physical properties and technological applications. Acta Biomater. *10*, 1671–1682.

12. Cornwell, D.J., and Smith, D.K. (2015). Expanding the scope of gels – combining polymers with low-molecular-weight gelators to yield modified self-assembling smart materials with high-tech applications. Mater. Horiz. *2*, 279–293.

13. Okesola, B.O., and Smith, D.K. (2016). Applying low-molecular weight supramolecular gelators in an environmental setting – self-assembled gels as smart materials for pollutant removal. Chem. Soc. Rev. *45*, 4226–4251.

14. Escuder, B., Rodríguez-Llansola, F., and Miravet, J.F. (2010). Supramolecular gels as active media for organic reactions and catalysis. New J. Chem. *34*, 1044–1054.

15. Weiss, R.G. (2014). The past, present, and future of molecular gels. What is the status of the field, and where is it going? J. Am. Chem. Soc. *136*, 7519–7530.

16. Mears, L.L.E., Draper, E.R., Castilla, A.M., Su, H., Zhuola, Dietrich, B., Nolan, M.C., Smith, G.N., Doutch, J., Rogers, S., et al. (2017). Drying affects the fiber network in low molecular weight hydrogels. Biomacromolecules *18*, 3531–3540.

17. Wang, Y., Qi, W., Wang, J., Li, Q., Yang, X., Zhang, J., Liu, X., Huang, R., Wang, M., Su, R., and He, Z. (2018). Columnar liquid crystals self-assembled by minimalistic peptides for chiral sensing and synthesis of ordered mesoporous silica. Chem. Mater. *30*, 7902–7911.

18. Du, X., Zhou, J., Shi, J., and Xu, B. (2015). Supramolecular hydrogelators and hydrogels: from soft matter to molecular biomaterials. Chem. Rev. *115*, 13165–13307.

19. Fleming, S., and Ulijn, R.V. (2014). Design of nanostructures based on aromatic peptide amphiphiles. Chem. Soc. Rev. *43*, 8150–8177.

20. Dasgupta, A., Mondal, J.H., and Das, D. (2013). Peptide hydrogels. RSC Adv. *3*, 9117–9149.

21. Draper, E.R., and Adams, D.J. (2019). Controlling the assembly and properties of low-molecular-weight hydrogelators. Langmuir *35*, 6506–6521.

22. Mahler, A., Reches, M., Rechter, M., Cohen, S., and Gazit, E. (2006). Rigid, self-assembled hydrogel composed of a modified aromatic dipeptide. Adv. Mater. *18*, 1365–1370.

23. Chen, L., Revel, S., Morris, K., Serpell, L.C., and Adams, D.J. (2010). Effect of molecular structure on the properties of naphthalene–dipeptide hydrogelators. Langmuir *26*, 13466–13471.

24. Li, J., Du, X., Hashim, S., Shy, A., and Xu, B. (2017). Aromatic–aromatic interactions enable α-helix to β-sheet transition of peptides to form supramolecular hydrogels. J. Am. Chem. Soc. *139*, 71–74.

25. Martin, A.D., Wojciechowski, J.P., Robinson, A.B., Heu, C., Garvey, C.J., Ratcliffe, J., Waddington, L.J., Gardiner, J., and Thordarson, P. (2017). Controlling self-assembly of diphenylalanine peptides at high pH using heterocyclic capping groups. Sci. Rep. *7*, 43947.

26. Martin, A.D., Robinson, A.B., Mason, A.F., Wojciechowski, J.P., and Thordarson, P. (2014). Exceptionally strong hydrogels through self-assembly of an indole-capped dipeptide. Chem. Commun. *50*, 15541–15544.

27. Ou, C., Zhang, J., Zhang, X., Yang, Z., and Chen, M. (2013). Phenothiazine as an aromatic capping group to construct a short peptide-based 'super gelator'. Chem. Commun. *49*, 1853–1855.

28. Zhou, Y., Cui, H., Shu, C., Ling, Y., Wang, R., Li, H., Chen, Y., Lu, T., and Zhong, W. (2015). A supramolecular hydrogel based on carbamazepine. Chem. Commun. *51*, 15294–15296.

29. Awhida, S., Draper, E.R., McDonald, T.O., and Adams, D.J. (2015). Probing gelation ability for a library of dipeptide gelators. J. Colloid Interface Sci. *455*, 24–31.

30. Wu, F.-Y., Hsu, S.-M., Cheng, H., Hsu, L.-H., and Lin, H.-C. (2015). The effect of fluorine on supramolecular hydrogelation of 4-fluorobenzyl-capped diphenylalanine. New J. Chem. *39*, 4240–4243.

31. Farahani, A.D., Martin, A.D., Iranmanesh, H., Bhadbhade, M.M., Beves, J.E., and Thordarson, P. (2019). Gel- and solid-state-structure of dialanine and diphenylalanine amphiphiles: importance of C•••H interactions in gelation. ChemPhysChem *20*, 972–983.

32. Houton, K.A., Morris, K.L., Chen, L., Schmidtmann, M., Jones, J.T.A., Serpell, L.C., Lloyd, G.O., and Adams, D.J. (2012). On crystal versus fiber formation in dipeptide hydrogelator systems. Langmuir *28*, 9797–9806.

33. Draper, E.R., Morris, K.L., Little, M.A., Raeburn, J., Colquhoun, C., Cross, E.R., McDonald, T.O., Serpell, L.C., and Adams, D.J. (2015). Hydrogels formed from Fmoc amino acids. CrystEngComm *17*, 8047–8057.

34. Adams, D.J., Morris, K., Chen, L., Serpell, L.C., Bacsa, J., and Day, G.M. (2010). The delicate balance between gelation and crystallisation: structural and computational investigations. Soft Matter *6*, 4144–4156.

35. Guterman, T., Levin, M., Kolusheva, S., Levy, D., Noor, N., Roichman, Y., and Gazit, E. (2019). Real-time in-situ monitoring of a tunable pentapeptide gel–crystal transition. Angew. Chem. Int. Ed. *58*, 15869–15875.

36. Smith, A.M., Williams, R.J., Tang, C., Coppo, P., Collins, R.F., Turner, M.L., Saiani, A., and Ulijn, R.V. (2008). Fmoc-diphenylalanine self assembles to a hydrogel via a novel architecture based on π–π interlocked β-sheets. Adv. Mater. *20*, 37–41.

37. Braun, H.-G., and Cardoso, A.Z. (2012). Self-assembly of Fmoc-diphenylalanine inside liquid marbles. Coll. Surf. B *97*, 43–50.

38. Jayawarna, V., Ali, M., Jowitt, T.A., Miller, A.F., Saiani, A., Gough, J.E., and Ulijn, R.V. (2006). Nanostructured hydrogels for three-dimensional cell culture through self-assembly of fluorenylmethoxycarbonyl–dipeptides. Adv. Mater. *18*, 611–614.

39. Eckes, K.M., Mu, X., Ruehle, M.A., Ren, P., and Suggs, L.J. (2014). β sheets not required: combined experimental and computational studies of self-assembly and gelation of the ester-containing analogue of an Fmoc-dipeptide hydrogelator. Langmuir *30*, 5287–5296.

40. van Esch, J.H. (2009). We can design molecular gelators, but do we understand them? Langmuir *25*, 8392–8394.

41. Dastidar, P. (2008). Supramolecular gelling agents: can they be designed? Chem. Soc. Rev. *37*, 2699–2715.

42. Melnichenko, Y.B., and Wignall, G.D. (2007). Small-angle neutron scattering in materials science: recent practical applications. J. Appl. Phys. *102*, 021101.

43. Chaudhuri, B.N. (2015). Emerging applications of small angle solution scattering in structural biology. Protein Sci. *24*, 267–276.

44. Bendedouch, D., Chen, S.H., and Koehler, W.C. (1983). Structure of ionic micelles from small angle neutron scattering. J. Phys. Chem. *87*, 153–159.

45. Sanchez-Fernandez, A., Arnold, T., Jackson, A.J., Fussell, S.L., Heenan, R.K., Campbell, R.A., and Edler, K.J. (2016). Micellization of alkyltrimethylammonium bromide surfactants in choline chloride:glycerol deep eutectic solvent. Phys. Chem. Chem. Phys. *18*, 33240–33249.

46. Bush, M., Alhanshali, B.M., Qian, S., Stanley, C.B., Heller, W.T., Matsui, T., Weiss, T.M., Nicholl, I.D., Walz, T., Callaway, D.J.E., and Bu, Z. (2019). An ensemble of flexible conformations underlies mechanotransduction by the cadherin–catenin adhesion complex. Proc. Nat. Acad. Sci. U S A *116*, 21545–21555.

47. Laux, V., Callow, P., Svergun, D.I., Timmins, P.A., Forsyth, V.T., and Haertlein, M. (2008). Selective deuteration of tryptophan and methionine residues in maltose binding protein: a model system for neutron scattering. Eur. Biophys. J. *37*, 815–822.

48. Banc, A., Genix, A.-C., Dupas, C., Sztucki, M., Schweins, R., Appavou, M.-S., and Oberdisse, J. (2015). Origin of small-angle scattering from contrast-matched nanoparticles: a study of chain and filler structure in polymer nanocomposites. Macromolecules *48*, 6596–6605.

49. Yuan, G., and Hammouda, B. (2019). Solvent and polymer H/D isotope effects on miscibility in Poly(ethylene oxide)/Ethanol system. Polymer *166*, 178–183.

50. Cardoso, A.Z., Mears, L.L.E., Cattoz, B.N., Griffiths, P.C., Schweins, R., and Adams, D.J. (2016). Linking micellar structures to hydrogelation for salt-triggered dipeptide gelators. Soft Matter *12*, 3612–3621.

51. Chen, L., Pont, G., Morris, K., Lotze, G., Squires, A., Serpell, L.C., and Adams, D.J. (2011). Salt-induced hydrogelation of functionalised-dipeptides at high pH. Chem. Commun. *47*, 12071–12073.

52. Draper, E.R., Su, H., Brasnett, C., Poole, R.J., Rogers, S., Cui, H., Seddon, A., and Adams, D.J. (2017). Opening a can of worm(-like micelle)s: the effect of temperature of solutions of functionalized dipeptides. Angew. Chem. Int. Ed. *129*, 10603–10606.

53. Frederix, P., Patmanidis, I., and Marrink, S.J. (2018). Molecular simulations of self-assembling bio-inspired supramolecular systems and their connection to experiments. Chem. Soc. Rev. *47*, 3470–3489.

54. Iscen, A., and Schatz, G.C. (2017). Peptide amphiphile self-assembly. Europhys. Lett. *119*, 38002.

55. Bochicchio, D., and Pavan, G.M. (2018). Molecular modelling of supramolecular polymers. Adv. Phys. X *3*, 1436408.

56. Pocker, Y., and Green, E. (1973). Hydrolysis of D-glucono-.delta.-lactone. I. General acid-base catalysis, solvent deuterium isotope effects, and transition state characterization. J. Am. Chem. Soc. *95*, 113–119.

57. Adams, D.J., Butler, M.F., Frith, W.J., Kirkland, M., Mullen, L., and Sanderson, P. (2009). A new method for maintaining homogeneity during liquid–hydrogel transitions using low molecular weight hydrogelators. Soft Matter *5*, 1856–1862.

58. Wallace, M., Adams, D.J., and Iggo, J.A. (2013). Analysis of the mesh size in a supramolecular hydrogel by PFG-NMR spectroscopy. Soft Matter *9*, 5483–5491.

59. Draper, E.R., Wallace, M., Schweins, R., Poole, R.J., and Adams, D.J. (2017). Nonlinear effects in multicomponent supramolecular hydrogels. Langmuir *33*, 2387–2395.

60. Terech, P., Clavier, G., Bouas-Laurent, H., Desvergne, J.-P., Demé, B., and Pozzo, J.-L. (2006). Structural variations in a family of orthodialkoxyarenes organogelators. J. Colloid Interface Sci. *302*, 633–642.